Journal of Applied Sciences

ISSN 1812-5654

science alert

ANSInet
an open access publisher
http://ansinet.com

Journal of Applied Sciences 8 (18): 3129-3138, 2008
ISSN 1812-5654

Cyclic Strain Accumulation of Plain Stainless Steel Pressurized Cylinders Subjected to Dynamic Bending Moment

[1]M. Zehsaz, [1]S.J. Zakavi, [2]H. Mahbadi and [3]M.R. Eslami
[1]Faculty of Mechanical Engineering, University of Tabriz, Tabriz, Iran
[2]Azad University, Central Tehran Branch, Tehran, Iran
[3]Faculty of Mechanical Engineering, Amirkabir University of Technology, Tehran, Iran

Abstract: A series of 6 tests have been conducted using cylindrical specimens having mean diameter/thickness ratios in the range $8 \le D_m/t \le 28$. Each cylinder is pressurized up to its calculated design pressure and is loaded with an alternative bending moment at frequencies typical of seismic events simultaneously. Ratchetting of the cylinder wall has been observed and recorded in the hoop direction. A finite element analysis with the nonlinear isotropic/kinematic (combined) hardening model has been used to evaluate ratchetting behavior of the cylinder under mentioned loading condition. The finite element results are compared with those obtained from experimental set-up. The results show that initial the rate of ratchetting is large and then it decreases with the increasing of cycles. The results also show that the FE method and analytical solutions give over estimated values comparing with the experimental data.

Key words: Ratchetting, pressurized pipes, cyclic bending moment, seismic loading, strain hardening, finite element

INTRODUCTION

The literature review shows that accurate closed form solutions may not be found to analyse the ratchetting behavior of the pressurized pipes under cyclic bending loading which can be caused by seismic loads. However, approximate solutions have been developed by Mahbadi and Eslami (2006), Abdel-Karim (2005), Chen *et al.* (2005), Johansson *et al*., (2005), Chen and Jiao (2004), Bari and Hassan (2000, 2001, 2002), Abdel-Karim and Ohno (2000), Chaboche (1991, 1994) and Beaney (1990, 1991) which can be used to calculated the induced incremental plastic strains caused by ratchetting. Experimental works to study the ratchetting of the straight pipes have also been carried out by the EPRI (Ranganath *et al*., 1989; English, 1988).

The kinematic hardening theory of plasticity based on the Armstrong-Frederick model is used by Mahbadi and Eslami (2006) to evaluate the cyclic loading behavior of thick cylindrical vessels. The results found from their numerical analysis shows that the when the stress range is more than twice the yield stress, kinematic hardening theory with the Armstrong-Frederick model excluding creep, predicts ratchetting for load controlled cyclic loading while shakedown is predicted for deformation controlled cyclic loading. Kinematic hardening theory with the Prager model predict shakedown for load and deformation controlled cyclic loading of thick vessels (Eslami and Mahbadi, 2001).

The work reported here is based on a series of tests conducted using specimens, having $8 \le D_m/t \le 28$. There is notable dearth of information available which seeks to compare experimental data such as that reported in references (Moreton *et al*., 1994, 1996, 1998a, b), with finite element computations. This is surprising since it is well known that analytical solutions (such as those presented in references (Beaney, 1990) differ with experimental data by several orders of magnitude. It is of paramount importance to establish reliable theoretical methods for predicting ratchetting rates and the use of Finite Element (FE) codes would seem to be a logical way forward. Therefore, in this study a finite element analysis with the nonlinear isotropic/kinematic (combined) hardening model is used to evaluate ratchetting behavior of plain stainless steel pressurized cylinders subjected to dynamic bending moment.

MATERIALS AND METHODS

In this study, a finite element code, ABAQUS, was used to study the ratchetting of plain stainless steel pressurized pipes subjected to cyclic bending loading.

Corresponding Author: M. Zehsaz, Faculty of Mechanical Engineering, University of Tabriz, Tabriz, Iran

Firstly, a series of tests has been undertaken subjecting pressurized pipe specimens to rising amplitude dynamic (5 Hz, the resonant frequency) bending moments. Secondly, by conducting a series of finite element runs based on nonlinear isotropic/kinematic hardening model using the ABAQUS, the experimental tests have been modeled and ratchetting data obtained. The two sets of results are compared with each other and with the analytical models of references (Beaney, 1990).

HARDENING MODEL

The isotropic and kinematic hardening models are used to simulate the inelastic behavior of materials that are subjected to cyclic loading. The use of plasticity material models with isotropic type hardening is generally not recommended since they will continue to harden during cyclic loading. The isotropic hardening model always predicts shakedown behavior, if creep is not considered. Kinematic hardening plasticity models are proposed to model the inelastic behavior of materials that are subjected to repeated loading. For example, The Armstrong-Frederick kinematic hardening model is suggested for the nonlinear strain hardening materials. The results of these models are discussed for structures under various types of cyclic loads in references (Mahbadi and Eslami, 2006; Eslami and Mahbadi, 2001; Prager, 1956).

A kinematic hardening model or a (combined) nonlinear isotropic/kinematic hardening model may be used to simulate the behavior of materials that are subjected to cyclic loading. The evolution law in these models consists of a kinematic hardening component which describes the translation of the yield surface in stress space. An isotropic component which describes the change of the elastic range is added for the nonlinear isotropic/kinematic hardening model.

Isotropic hardening model: The isotropic hardening model which describes the change of the elastic range is discussed here. Isotropic hardening means that the yield surface changes size uniformly in all directions such that the yield stress increases in all stress directions as plastic straining occurs.

According to the isotropic hardening model, the yield function is generally expressed as (Lubliner, 1990):

$$f(\sigma_{ij}, T, \xi_i) = 0 \tag{1}$$

where, ξ_i is the internal variable tensor. If we assume that the material constant are independent of temperature, Eq. 1 may be rewritten in the form:

$$f(\sigma_{ij}) = k(\xi_i) \tag{2}$$

where, k is a non-negative constant being function of the internal variable tensor ξ_i. The mathematical meaning of Eq. 2 is that the center of yield surface in the stress space will not change as the result of loading or unloading, but its distance from the coordinate origin change as the internal variable ξ_i change.

The flow rule associated with the yield function (2) has the general form (Mendelson, 1960)

$$d\varepsilon_{ij}^{P} = d\lambda \frac{\partial f}{\partial \sigma_{ij}} \tag{3}$$

where, $d\lambda$ is a non-negative constant and function of the internal variable ξ_i. The constant $d\lambda$ is defined in terms of the effective stress and the increment of effective plastic strain.

For Von-Mises yield criterion Eq. 3 is (Mendelson, 1960):

$$d\varepsilon_{ij}^{P} = \frac{3}{2}\frac{d\varepsilon_P}{d\sigma_e} S_{ij} \tag{4}$$

where, S_{ij} is the deviator stress tensor, $d\varepsilon_P$ is the increment of effective plastic strain and σ_e is the effective stress defined as (Mendelson, 1960):

$$S_{ij} = \sigma_{ij} - \delta_{ij}\sigma_m \tag{5}$$

$$\sigma_m = \frac{1}{3}(\sigma_1 + \sigma_2 + \sigma_3) \tag{6}$$

$$d\varepsilon_P = \sqrt{\frac{2}{3}[(d\varepsilon_1^P - d\varepsilon_2^P)^2 + (d\varepsilon_2^P - d\varepsilon_3^P)^2 + (d\varepsilon_3^P - d\varepsilon_1^P)^2]} \tag{7}$$

Kinematic hardening model: The classical linear kinematic hardening rule and different nonlinear kinematic hardening models are available for the plastic analysis of structures. The nonlinear kinematic hardening model was first proposed by Armstrong-Frederick (1966). Nonlinearities are given as a recall term in the Prager rule. So that the transformation of yield surface in the stress space is different during loading and unloading. This is done by assuming different hardening modulus in loading and unloading conditions.

The yield function for rate independent plasticity is expressed as:

$$f(\sigma_{ij}, T, \xi_k) = 0 \qquad i,j = 1,2,3 \qquad k = 1,2,3...,m \tag{8}$$

with the evolution equations of

$$g_k(\sigma_{ij}, T, \xi_k) = 0 \qquad i,j = 1,2,3 \qquad k = 1,2,3 \tag{9}$$

where, ξ_k is the internal variable tensor. Assuming that the material constants are independent of temperature, Eq. 8 for the Von-Mises yield criterion may be rewritten in the form (Mahbadi and Eslami, 2006)

$$f(\sigma_{ij} - \alpha_{ij}) = [\frac{3}{2}(s_{ij} - a_{ij}).(s_{ij} - a_{ij})]^{\frac{1}{2}} = \sigma_0 \quad (10)$$

where σ_{ij} and α_{ij} are the stress and back stress tensors and s_{ij} and a_{ij} are the stress and back stress deviatoric tensors in the stress space. If the plastic strain ε_{ij}^p and the back stress tensor α_{ij} are assumed as the internal variables, the evolution equations are:

(I) Flow rule:

$$d\varepsilon_{ij}^P = \frac{1}{H}\left\langle \frac{\partial f}{\partial \sigma_{ij}} d\sigma_{ij} \right\rangle \frac{\partial f}{\partial \sigma_{ij}} \quad (11)$$

(II) Armstrong-Frederick kinematic hardening model:

$$da_{ij} = \frac{2}{3} C d\varepsilon_{ij}^P - \gamma a_{ij} |d\varepsilon_P| \quad (12)$$

where, C and γ are two material constants in the Armstrong-Frederick kinematic hardening model and they will be found from the uniaxial strain controlled stable hysteresis curve. Assuming that during the loading $d\varepsilon_P$ is positive, since $da_x = d\sigma_x$, Eq. 12 for the uniaxial load changes to the following form:

$$H = \frac{d\sigma_x}{d\varepsilon_x^P} = \frac{d\alpha_x}{d\varepsilon_x^P} = C - \gamma\alpha_x \quad (13)$$

Solution of differential Eq. 13 for α_x yields

$$\alpha_x = \frac{C}{\gamma} + c_0 \exp(-\gamma\varepsilon_x^P) \quad (14)$$

where, c_0 is the constant of integration. The trace of α_x begins from -C/γ at $-\varepsilon_1^P$. Which corresponds to the starting point of the strain controlled stable hysteresis loop (Armstrong and Frederick, 1966). Using the condition, the constant c_0 is found and Eq. 14 for the positive $d\varepsilon_x^P$ (tensile plastic strain increment) may be rewritten as:

$$\alpha_x = \frac{C}{\gamma} - \frac{2C}{\gamma} \exp[-\gamma(\varepsilon_x^P + \varepsilon_1^P)] \quad (15)$$

If during loading the value of $d\varepsilon_x^P$ is negative (compressive plastic strain increment), then Eq. 13 and 15 changes to:

$$H = C + \gamma\alpha_x \quad (16)$$

$$\alpha_x = -\frac{C}{\gamma} + \frac{2C}{\gamma} \exp[-\gamma(-\varepsilon_x^P + \varepsilon_1^P)] \quad (17)$$

However, this model provides an anisotropy effect in tension/compression curve due to the nonlinearity of the trace of α_x.

Nonlinear isotropic/kinematic (combined) hardening model: In the kinematic hardening models the center of the yield surface moves in stress space due to the kinematic hardening component. In addition, when the nonlinear isotropic/kinematic hardening model is used, the yield surface range may expand due to the isotropic component. These features allow modeling of inelastic deformation in metals that are subjected to cycles of load or temperature, resulting in significant inelastic deformation and, possibly, low-cycle fatigue failure.

The evolution law of this model consists of two components: a nonlinear kinematic hardening component, which describes the translation of the yield surface in stress space through the backstress α and an isotropic hardening component, which describes the change of the equivalent stress defining the size of the yield surface, as σ^0 a function of plastic deformation.

The kinematic hardening component is defined to be an additive combination of a purely kinematic term (linear Ziegler hardening law) and a relaxation term (the recall term), which introduces the nonlinearity. When temperature and field variable dependencies are omitted, the hardening law is:

$$\dot{\alpha} = C\frac{1}{\sigma^0}(\sigma - \alpha)\dot{\bar{\varepsilon}}^p - \gamma\alpha\dot{\bar{\varepsilon}}^p \quad (18)$$

where, C and γ are material parameters that must be calibrated from cyclic test data. C is the initial kinematic hardening modulus and γ determines the rate at which the kinematic hardening modulus decreases with increasing plastic deformation. The kinematic hardening law can be separated into a deviatoric part and a hydrostatic part; only the deviatoric part has an effect on the material behavior. When C and γ are zero, the model reduces to an isotropic hardening model. When γ is zero, the linear Ziegler hardening law is recovered.

The isotropic hardening behavior of the model defines the evolution of the yield surface size, σ^0 as a function of the equivalent plastic strain $\bar{\varepsilon}^p$. This evolution can be introduced by specifying σ^0 as a function of $\bar{\varepsilon}^p$ by using the simple exponential law

$$\sigma^0 = \sigma|_0 + Q_\infty(1 - e^{-b\bar{\varepsilon}^p}) \quad (19)$$

where, $\sigma|_0$ is the yield stress at zero plastic strain and Q_∞ and b are material parameters. Q_∞ is the maximum change in the size of the yield surface and b defines the rate at which the size of the yield surface changes as plastic straining develops. When the equivalent stress defining the size of the yield surface remains constant $\sigma^0 = \sigma|_0$, the model reduces to a nonlinear kinematic hardening model.

REVIEW OF BEANEY METHOD

Beaney undertook experimental work on both plain pipes and a range of pipework components. Only his work on plain pipes will be discussed here. His test pipes (austenitic and ferritic) having diameters between 25.4 and 89 mm were shaken at each end by hydraulic actuators at a fundamental natural frequency of about 5 Hz. Most of the pipes were pressurized to their nominal design pressure of about 2/3 of the yield. The pipes were strain gauged and data acquisition and processing system provided. Beaney (1991) found that the most notable observation from his tests was that the level of resonant vibration was self-limiting. As the input amplitude increased, yielding started to occur in the pipe wall and this yielding absorbed energy and hence limited the bending moment that the pipe could sustain. It was noted that unpressurized pipework did not fail even when excessively high input accelerations were applied at the supports. The predicted level of input accelerations during an earthquake is typically about 0.25 g and accelerations as high as 5 g were used in these tests. The pressurized pipes exhibited hoop ratchetting both in the plain pipe and at areas of local stress concentration. In some tests failure occurred in as few as 40 cycles when the hoop strains which developed exhausted the ductility of the material (Fig. 1).

In 1986 Beaney attempted to quantify the ratchet strain by modifying the Edmunds and Beer relationship by using the more accurate Mises yield criterion but retaining the assumption of elastic/perfectly plastic material behavior.

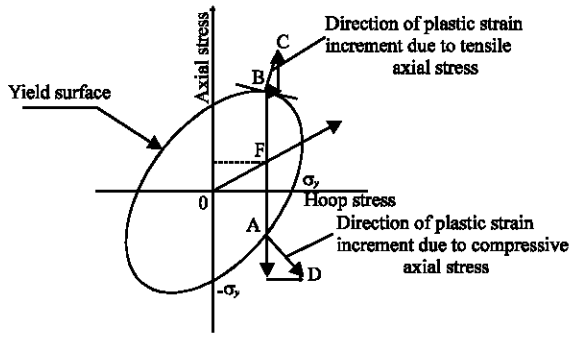

Fig. 1: Von mises yield surface

Edmunds and Beer gave the ratchet strain in the hoop direction as:

$$\varepsilon_\theta^R = \frac{3\sigma_\theta}{E}\left[\frac{2\varepsilon_\phi E}{2\sigma_y - \sigma_\theta} - 1\right] \quad (20)$$

where, σ_θ is the hoop stress (due to pressure), ε_ϕ is the applied dynamic strain amplitude, σ_y is the yield stress and E is the Young's modulus.

Clearly one problem in using this relationship is in estimating the applied dynamic strain amplitude. Beaney (1990) suggested that this equation could be written as:

$$\varepsilon_\theta^R = \frac{6\sigma_\theta}{E(2\sigma_y - \sigma_\theta)}\left[\{\sigma_\phi + \frac{\sigma_\theta}{2}\} - \sigma_y\right] \quad (21)$$

where, σ_φ is the axial stress amplitude. For, $\varepsilon_\theta^R = 0$ Eq. 21 reduces to:

$$\frac{\sigma_\phi}{\sigma_{0.2}} = 1 - \frac{\sigma_\theta}{2\sigma_{0.2}} \quad (22)$$

Beaney commented that it was important to use the dynamic yield stress. However, for strain-hardening materials he found the static 0.2% proof stress a good substitute. For ferritic steels a good estimate of the dynamic yield stress could be made by noting that as soon as yielding occurs so does ratchetting. By observing the axial strain amplitude at the onset of ratchetting the maximum elastic stress σ could be calculated and thus the yield stress σ_y calculated, for various pipe pressures, using the expression he derived earlier (Moreton *et al*., 1994). That is:

$$\sigma_y = \sqrt{\sigma^2 + \sigma_\theta^2} \quad (23)$$

where, σ_θ is the hoop stress (due to pressure), σ_y is the dynamic yield stress and σ is the maximum elastic axial stress.

REVIEW OF EXPERIMENTAL ARRANGEMENT

The experimental arrangements used for testing plain cylinders and other pressurized piping components have been detailed previously (Yahiaoui *et al*., 1992). It is sufficient to give a brief outline of the technique.

Cylindrical specimens were machined from stainless steel bar stock to the form illustrated in Fig. 2. In order to minimize any residual stresses, these specimens were machined 1.5 mm oversize on all dimensions. These blanks were stress relived at 650°C (1 h + furnace cool). The bores of all specimens were reamed to 30 mm diameter and the outside surface profiled using a CNC (computer numeric controlled) lathe while holding the specimen on

Table 1: Specimen $8 \leq D_m/t \leq 28$ ratios

Specimen no.	Dimension A(mm)	t(mm)	D_m/t
SS1	38.57	4.285	8
SS2	35.46	2.73	12
SS3	34.00	2.00	16
SS4	33.16	1.58	20
SS5	32.60	1.30	24
SS6	32.22	1.11	28

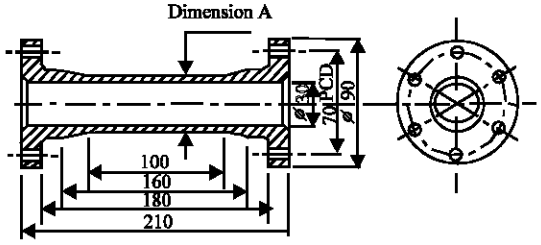

Fig. 2: The test specimen-All dimensions in mm

a mandrel. Six holes were provided in each end flange using the powered axial tooling of the CNC lathe. A total of six specimens were machined in this way and the dimension A was varied to provide the D_m/t ratios detailed in Table 1.

Strain gauges were bonded to the top and bottom surfaces using M-Bond AE 10 curing for 4 h at 30°C and 2 h at 100°C. Two-element, 90 rosettes were used to provide strain measurement in the hoop and axial directions. The gauge type selected was EA-06-125TM-120 from Micro measurements.

Tensile test specimens were taken axially from the bar stock. These were subjected to the same oversize machining, heat treatment and final machining stages as the cylindrical specimens. Tensile test showed that the linear part of the curve extended up to about 180 MPa and then strain-hardened significantly up to 76% strain with an ultimate stress of 565 MPa. Using the ASME III, Boiler and Pressure Vessel Code (Section III, Subsection NB), the allowable design stress intensity S_m was determined as:

$$S_m = \text{Min}\left(\frac{1}{3}\sigma_{ult}, \frac{2}{3}\sigma_y\right) \quad (24)$$

A typical stress-strain curve is included in Fig. 3. It should be noted that all values of stress given above and in Fig. 3 are engineering stress. The rig used to provide simulated seismic bending is illustrated in Fig. 4. This is a 250 kN servohydraulic testing machine fitted with a fatigue module. The test specimen was attached to extension limbs (via the flanged connections) and mounted in roller bearing supports outboard of the flanged connections. Tuning weights were added to the

Table 2: Material properties obtained by tensile test

200 GPa	Young's modulus
565 MPa	Ultimate stress
242 MPa	2% Proof stress
81%	Elongation at failure (%)
161 MPa	$S_m = \min(\sigma_{ult}/3, 2\sigma_Y/3)$

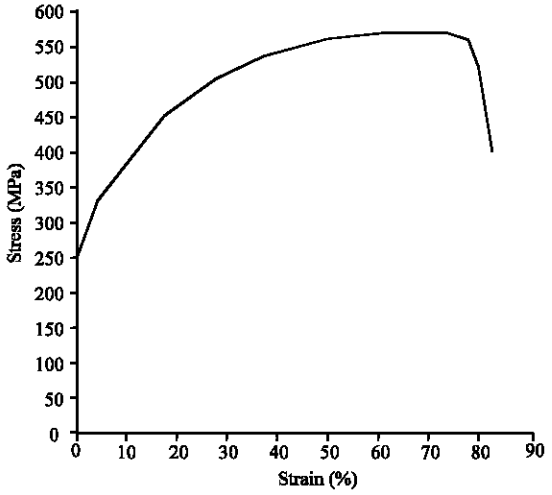

Fig. 3: Stress-strain curve for the stainless steel used to manufacture the tubular specimens

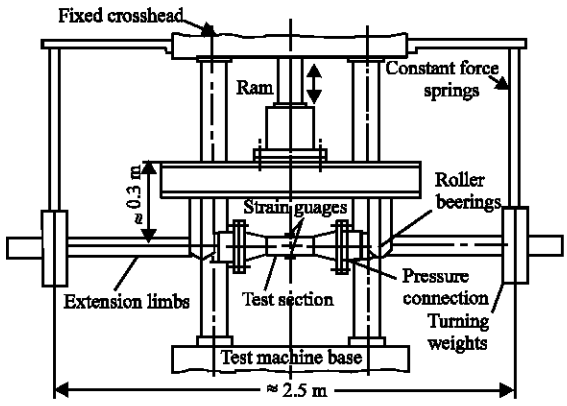

Fig. 4: The seismic test rig

ends of the extension limbs which were supported on constant force springs to eliminate any gravity stresses. Excitation of the test machine crosshead thus caused large-amplitude vibration of the test pipework. Frequency sweeps at elastic amplitudes allowed the natural frequency to be established and to confirm the amplitude of vibration to be the same on each side of the rig. The bending moment experienced by the test specimen was extrapolated from moment measurements made in the elastic region of the extension limbs.

The design pressure for each cylinder was calculated using the ASME III code which gives:

$$P_d = \frac{2S_m t}{D_0 - 2yt} \quad (25)$$

with S_m = 161 MPa (Table 2) and y = 0.4

All specimens were tested using a rising amplitude technique; i.e., having mounted the specimen in the test rig, tuned the natural frequency and applied the test pressure, where small input amplitude was applied and maintained for about 20 sec. During this time a high-speed data logger was used to record the input displacement, all strain gauge readings and the output acceleration provided by an accelerometer positioned on one of the tuning weights. Having completed such a test, the amplitude of vibration was increased and the process repeated. At high input amplitudes the duration of the test was reduced because of the limited stored hydraulic capacity of the testing machine.

FINITE ELEMENT ARRANGEMENT

For all specimens the nonlinear finite element code, ABAQUS, was used to study ratchetting of straight pressurized pipe subjected to simulated seismic bending moments.

The cylindrical specimen model under pressure and cyclic bending moment is shown in Fig. 5. The simulation assembly was a 2.30 m long pipework modeled by 23 elements. The central test section was 3 elements long and the lateral extension limbs 10 elements long. Each element used 18 integration points around the pipe and four Fourier (or ovalization) modes. In the radial direction, 7 and 9 integration points through the thickness were used for the thin- and thick- walled models, respectively. The latter numbers of integration points were decided after a series of solution convergence runs. In the analysis, the load reactions were simulated by applying boundary conditions at nodes 11 and 14 of the model. The latter nodes are the ends of the three elements making up the central test section. The displacements in all three directions and twisting about the pipe axis were prevented at these nodes. The additional boundary condition along the pipe axis was to simulate the closed end axial force reaction due to the internal pressure.

The most accurate element in the ABAQUS code for this type of structural system considering beam elements, pipe elements and elbow elements is the elbow element. Four types of elbow elements are available in the ABAQUS library, of which the two-noded element ELBOW 31B was found to give the best results. Although these elbow elements appear like beam elements, they are actually elements where shell theory is used to model the behavior. Element type ELBOW 31B is cheaper (in computational time) than the standard ELBOW 31 and

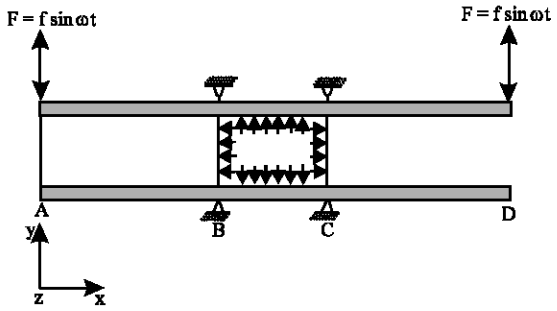

Fig. 5: Cylindrical specimen model under pressure and cyclic bending moment

ELBOW 32 elements. It uses a simplified formulation where only ovalization is considered. Both warping and axial gradients of the ovalization are neglected.

The loading was applied in two stages. First the internal pressure, set at the design value of the pipe, was applied and held constant for the remainder of the analysis. Next, the dynamic load to induce the cyclic bending was applied at the end nodes of the simulation model. It was specified as a sinusoidal force with a circular frequency as obtained from the simulation test. Because of the dynamic nature of the analysis which induces different inertia loads due to the distributed weight of the lateral extension limbs as the vertical displacement frequency and amplitude were increased, the amplitude of the excitation had to be carefully adjusted until an equivalent moment equal to the value obtained during testing was achieved.

The results gained experimentally and from FE analyses using nonlinear isotropic/kinematic (combined) hardening model (with C = 1.907 GPa and γ = 5.78) are detailed below. Also, included is the result obtained using the Beaney (1990) analysis.

EXPERIMENTAL AND THEORETICAL RESULTS

Detailed results will be presented for two of the specimens tested (SS2 and SS6) and summary results will be given for all tests conducted. It is perhaps useful to present, firstly, the bending moment response obtained experimentally (Fig. 6a) and by the FE analysis (Fig. 6b). These clearly show that a reasonably stable bending moment response has been achieved for the duration of the test- in this case up to 10 sec.

Strain gauges and a high-speed data capture system were used to record the experimental hoop and axial strains developed on the top and bottom surfaces of the seismic specimens. A FORTRAN routine was written to reconstruct the form of the strain signal and this is presented for the top surface hoop strain gauge of specimen SS2 in Fig. 7a. The experimentally obtained axial

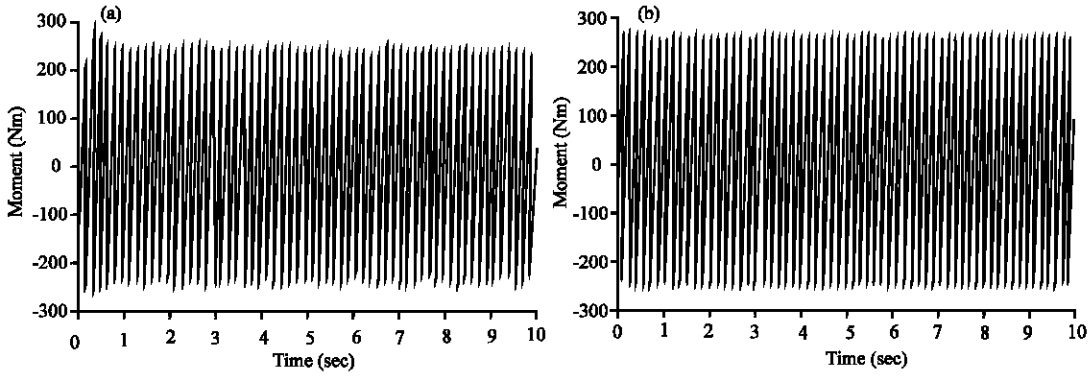

Fig. 6: (a) Experimental dynamic bending moment responses and (b) FE analysis dynamic bending moment responses

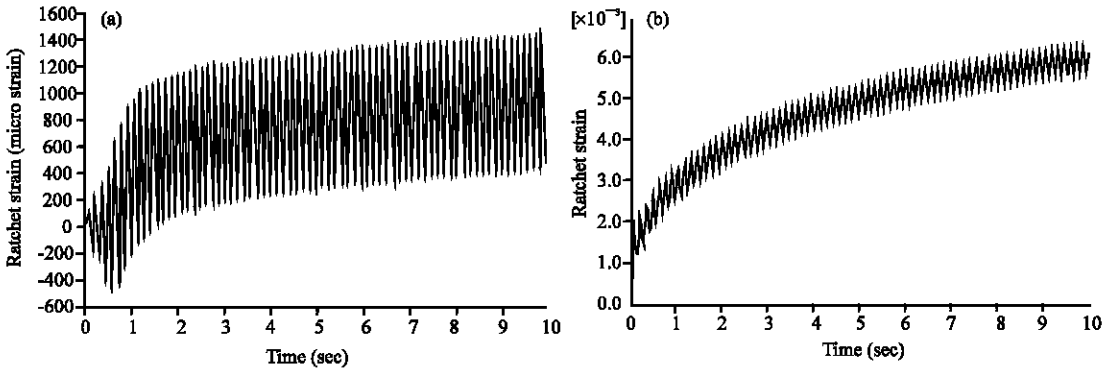

Fig. 7: (a) Experimental hoop strain data for the top surface of specimen SS2 at a dynamic bending moment of 582.45 Nm ($M/M_{0.2}$) = 1.15 and (b) Hoop strain data using FE analysis for the true stress-strain curve and combined hardening for the top surface of specimen SS2 at a dynamic bending moment of 582.45 Nm ($M/M_{0.2}$) = 1.15

strain was found to be constant throughout the test and thus no data for these gauges has been included. The hoop strain data extracted from the FE analysis for the top surface of the cylinder are presented in Fig. 7b.

All of the experimental ratchetting results for the tests and from FE analysis on specimens SS1 to SS6 are plotted in Fig. 8a and b, respectively. Here, the strain for each cycle has been calculated as the average over the period of the test and plotted against $M/M_{0.2}$. Figure 8a and b show the data recorded for the bottom surface.

The response of the specimens during these tests is illustrated in Fig. 9. The dynamic bending moment experienced by the specimen has been plotted against the input displacement for each of the specimens SS1 to SS6.

Although there is some evidence in this plot that the dynamic bending moments do approach a self-limiting value, this is much less distinct than has been seen in previous works (Moreton *et al*., 1996; Beaney, 1990).

A typical set of results for specimen SS6 is shown in Fig 10, which includes results from the FE analysis using with the combined hardening model. Here, the ratchet strain per cycle averaged over the first 20 sec of excitation has been plotted against increasing $M/M_{0.2}$ ratios for the experimentally obtained data, the finite element data and the Beaney (1990) analytical solution ($M_{0.2}$ is moment based on proof stress $\sigma_{0.2}$ = 242 MPa). For both experimental data and the finite element results, the averages of the top and bottom surface ratchet strains are shown. The same information obtained for specimen SS2 is illustrated in Fig. 11.

Figure 12 illustrates the nature of this failure for typical specimen of mild steel which appears to be a combination of hoop ratcheting (leading to the gross local swelling of the cylinder) and fatigue causing the hoop crack. Figure 13 shows the nature of this failure for typical stainless steel specimen. The ductility of the stainless steel used is very much greater than mild steel. Fig. 12 and 13 shown that the stainless steel specimens do not have any greater fatigue life than the mild steel specimens. Swelling in stainless steel is less than the mild steel.

It is evident from Fig. 7a, b, 10 and 11 that the hoop strain ratcheting rates predicted by the Beaney analysis and the FE analysis are very much greater than that found experimentally. In Table 3, the ratchet strains found

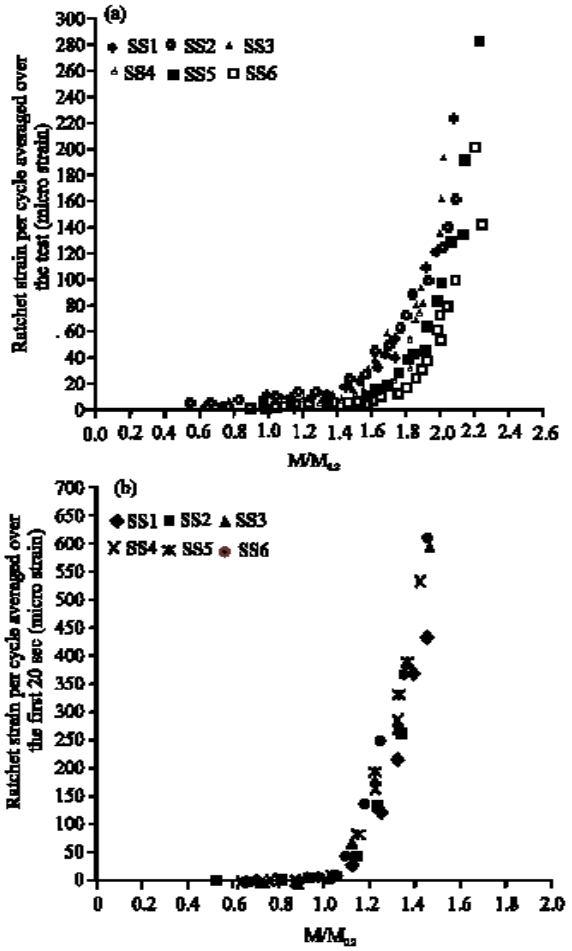

Fig. 8: (a) Experimental ratchetting data recorded on the bottom surface of specimens SS1 to SS6 and (b) Ratchetting data using FE analysis on the bottom surface of specimens SS1 to SS6

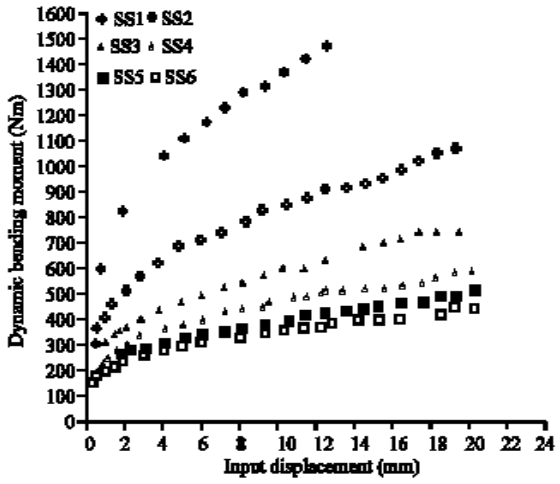

Fig. 9: Dynamic bending moment against the input displacement for each of the specimens SS1 to SS6

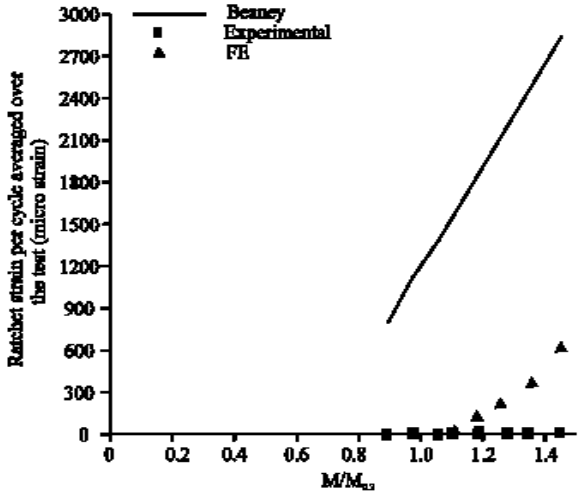

Fig. 10: Experimental, FE (Combined hardening) and Beaney ratchet strains for specimen SS6

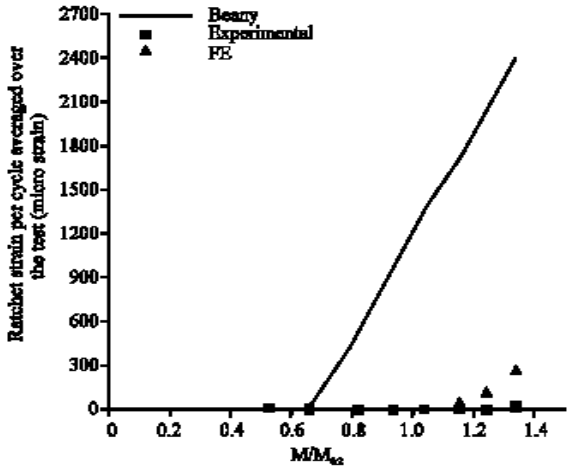

Fig. 11: Experimental, FE (combined hardening) and Beaney ratchet strains for specimen SS2

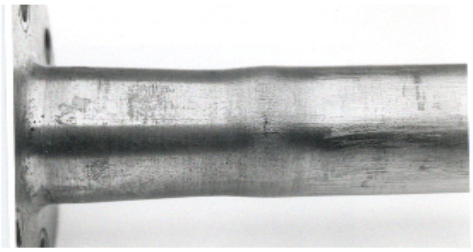

Fig. 12: Swelling in mild steel specimen

experimentally over a 20 sec test period and by FE analysis, for the same period, for specimen SS6 are summarized. The strains recorded on the top and bottom surfaces were found to be significantly different. In

Table 3: Experimental, analysis and FE ratchetting data for specimen SS6

Dynamic bending moment M (N m)	$M/M_{0.2}$	Beaney ratchet rate per cycle ($\mu\varepsilon$ cycle^{-1})	Experimental ratchet rate at first cycle ($\mu\varepsilon$ cycle^{-1})	Experimental ratchet rate averaged over the test ($\mu\varepsilon$ cycle^{-1})	FE (combined) ratchet rate averaged over the first 20 sec ($\mu\varepsilon$ cycle^{-1})
172.25	0.89	787.99	24	1.51(20)	1.13
191.00	0.98	1134.86	30	1.11(20)	4.87
204.95	1.06	1392.94	39	1.06(20)	10.61
213.50	1.10	1551.11	53	0.83(20)	42.70
228.90	1.18	1836.61	72	1.82(20)	140.05
242.10	1.25	2082.21	82	1.48(20)	246.26
263.90	1.36	2483.51	100	4.17(20)	367.91
283.15	1.46	2839.64	183	4.39(20)	603.56

Columns 4, 5 are the average of the top and bottom surface strains, Data obtained for P = P_d = 11.21 MPa, $M_{0.2}$ was based on proof stress $\sigma_{0.2}$ = 242 MPa Figures in parentheses in column five indicate the duration of the test in seconds at a testing frequency of 5.76 Hz

Table 4: Experimental, analysis and FE ratchetting data for specimen SS2

Dynamic bending moment M (N m)	$M/M_{0.2}$	Beaney ratchet rate per cycle ($\mu\varepsilon$ cycle^{-1})	Experimental ratchet rate at first cycle ($\mu\varepsilon$ cycle^{-1})	Experimental ratchet rate averaged over the test ($\mu\varepsilon$ cycle^{-1})	FE (combined) ratchet rate averaged over the first 20 sec ($\mu\varepsilon$ cycle^{-1})
271.45	0.53	0.00	22	1.99(20)	0.00
334.95	0.66	0.00	15	2.35(20)	0.00
415.25	0.82	533.19	33	3.88(20)	1.10
475.25	0.94	953.67	37	3.56(20)	2.48
530.60	1.04	1341.56	80	4.44(20)	7.20
582.45	1.15	1704.93	100	7.04(20)	42.82
632.45	1.24	2055.33	127	8.89(20)	135.30
680.10	1.34	2389.26	200	9.73(20)	263.17

Columns 4, 5 are the average of the top and bottom surface strains, Data obtained for P = P_d = 26.10 MPa ($P/P_{0.2}$ = 0.66), $M_{0.2}$ was based on proof stress $\sigma_{0.2}$ = 242 MPa, Figs. in parentheses in column five indicate the duration of the test in seconds at a testing frequency of 7.26 Hz

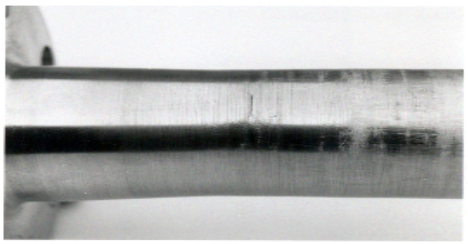

Fig. 13: Swelling in stainless steel specimen

Table 3, the average of these two surface strains is presented. Table 4 gives the equivalent information for the specimen SS2.

RESULTS AND DISCUSSION

The experimental work reported here provides reliable data which can be used to judge the value of the available analytical solution (Beaney, 1990) and FE analysis using the ABAQUS package. However, it should be noted that the experimental work used a rising amplitude technique which may effectively reduce the ratchet strain at any particular dynamic bending moment. It is possible that those tests conducted at low amplitude will harden the material sufficiently to reduce the ratchet strains observed at higher amplitudes. It is not possible to quantify the possible magnitude of this effect. This possible effect would not have influenced the dynamic bending moment at which ratchetting was first observed. Typical data obtained experimentally and from FE model for specimens SS1 to SS6 on the bottom surface are shown in Fig. 8a and b. Also Fig. 8a and b indicate that some ratchetting was observed at ratios of $M/M_{0.2}$ between 0.8 and 1.0 for the thinnest specimen SS6. Complete sets of data for specimens SS6 and SS2 are plotted in Fig. 10 and 11, respectively.

The important conclusion of this paper is to show the properties of nonlinear isotropic/kinematic hardening model to predict the cyclic loading behavior of the structures. Both experimental results and the FE analysis agree that ratcheting is influenced by the material stress-strain curve and load history. The rate of ratchetting depends significantly on the magnitude of the internal pressure and tangent modulus of the bilinear material. The results show that initial the rate of ratchetting is large and then it decreases with the increasing of cycles. The FE model predicts the hoop strain ratchetting rate to be greater than that found experimentally. The ratchetting rate predicted by the Beaney equation for all specimens overestimates the experimental rate. The results also show that the FE method and analytical solutions give over estimated values comparing with the experimental data.

ACKNOWLEDGMENTS

Appreciation is expressed to the technical staff of the Applied Mechanics Division of the Department of Mechanical Engineering at the University of Tabriz (Iran) and University of Liverpool (UK) for their assistance with the work.

NOTATION

t = Cylinder thickness
D_m = Cylinder mean diameter
D_0 = Cylinder outside diameter
E = Young's modulus
M = Dynamic bending moment
M_y = Yield moment
P = Internal pressure
P_d = Design pressure
P_y = Yield pressure
S_m = Allowable design stress intensity
y = Thickness correction factor = 0.4
ε_θ^R = Ratchet strain in the hoop direction
σ_{ult} = Tensile stress
σ_y = Yield stress
σ_θ = Hoop stress
θ_φ = Axial stress

REFERENCES

Abdel-Karim, M. and N. Ohno, 2000. Kinematic hardening model suitable for ratcheting with steady-state. Int. J. Plasticity, 16: 225-240.

Abdel-Karim, M., 2005. Numerical integration method for kinematic hardening rules with partial activation of dynamic recovery term. Int. J. Plasticity, 21: 1303-1321.

Armstrong, P.J. and C.O. Frederick, 1966. A mathematical representation of the multi axial Bauschinger effect. CEGB Report RD/B/N 731, Central Electricity Generating Board. The report is reproduced as a paper: 2007. Materials at High Temperatures, 24: 1-26.

Bari, S. and T. Hassan, 2000. Anatomy of coupled constitutive models for ratcheting simulation. Int. J. Plasticity, 16: 381-409.

Bari, S. and T. Hassan, 2001. Kinematic hardening rules in uncoupled modeling for multiaxial ratcheting simulation. Int. J. Plasticity, 17: 885-905.

Bari, S. and T. Hassan, 2002. An advancement in cyclic plasticity modeling for multiaxial ratcheting simulation. Int. J. Plasticity, 18: 873-894.

Beaney, E.M., 1990. Failure of pipework subjected to seismic loading. Nuclear Electric International Report, TD/B/6315/R90.

Beaney, E.M., 1991. Measurement of dynamic response and failure of pipework. Strain, 27: 88-94.

Chaboche, J.L., 1991. On some modifications of kinematic hardening to improve the description of ratcheting effects. Int. J. Plasticity, 7: 661-678.

Chaboche, J.L., 1994. Modeling of ratcheting: Evaluation of various approaches. Eur. Mech. A/Solids, 13: 501-518.

Chen, X. and R. Jiao, 2004. Modified kinematic hardening rule for multiaxial ratcheting prediction. Int. J. Plasticity, 20: 871-898.

Chen, X., R. Jiao and S.K. Kwang, 2005. On the Ohno-Wang kinematic hardening rules for multiaxial ratcheting modeling of medium carbon steel. Int. J. Plasticity, 21: 161-184.

English, W.F., 1988. Piping and fitting dynamic reliability program-fourth semi-annual progress report. Nov. 1986-Apr. 1987, GE Nuclear Energy, NEDC- 31542.

Eslami, M.R. and H. Mahbadi, 2001. Cyclic loading of thermal stress. J. Thermal Stress, 24: 577-603.

Johansson, G., M. Ekh and K. Runesson, 2005. Computational modeling of inelastic large ratcheting strains. Int. J. Plasticity, 21: 955-980.

Lubliner, J., 1990. Plasticity Theory. Facsimile Edn., Macmillian Pub. Co., ISBN-10: 0023721618 .

Mahbadi, H. and M.R. Eslami, 2006. Cyclic loading of thick vessels based on the prager and armstrong-frederick kinematic hardening models. Int. J. Pressure Vessels Piping, 83: 409-419.

Mendelson, A., 1960. Plasticity: Theory and Application. 1st Edn., R.E. Krieger Publ. Co., Malabar, Fla., ISBN: 0898745829.

Moreton, D.N., K. Yahiaoui, D.G. Moffat, H.C. Machin and L.A. Amesbury, 1994. The behavior of pressurized plain pipework subjected to simulated seismic loading. Strain J. BSSM., 30: 63-71.

Moreton, D.N., K.Yahiaoui, D.G. Moffat and M., Zehsaz, 1996. The effect of diameter/thickness ratio on the ratchetting behavior of pressurized plain pipework subjected to simulated seismic loading. Strain J. BSSM, 32: 91-96.

Moreton, D.N., M. Zehsaz, K. Yahiaoui and D.G. Moffat, 1998a. The ratchetting of plain carbon steel pressurized cylinders subjected to simulated seismic bending: The effect of the D/t ratio and component with finite element predictions. J. Strain Anal., 33: 39-53.

Moreton, D.N., M. Zehsaz, K. Yahiaoui and D.G. Moffat, 1998b. Ratchetting of plain pressurized pipework subjected to dynamic bending moments: Design code implications. Seismic Eng. ASME. PVP., 364: 83-98.

Prager, W., 1956. A new method of analyzing stresses and strains in work-hardening plastic solids. J. Applied Mech., 23: 493-496.

Ranganath, S., H. Hwang and S.W. Tagart, 1989. Piping and fitting dynamic reliability program. EPRI Nuclear Power Division.

Yahiaoui, K., D.G. Moffat and D.N. Moreton, 1992. Techniques for the investigation of the ratchetting behavior of piping components under internal pressure and simulated seismic loadings. Strain J. BSSM., 28: 53-59.